Available online at www.sciencedirect.com

ScienceDirect

Scripta Materialia 99 (2015) 1–4

Scripta MATERIALIA

www.elsevier.com/locate/scriptamat

# Atom probe study of chromium oxide spinels formed during intergranular corrosion

Alexandre La Fontaine,* Hung-Wei Yen, Peter J. Felfer, Simon P. Ringer and Julie M. Cairney

*School of Aerospace, Mechanical, Mechatronic Engineering, The University of Sydney, NSW 2006, Australia*
*Australian Centre for Microscopy and Microanalysis, The University of Sydney, NSW 2006, Australia*

Received 27 August 2014; revised 25 September 2014; accepted 25 September 2014
Available online 3 November 2014

Atom probe microscopy has been used to study the inhomogeneous nature of chromium oxide spinels in intergranular corrosion of a 253 MA austenitic stainless steel after thermal cycling up to 970 °C in air. The results indicate that the non-continuous character of the spinel layers originates from nanoscale phases such as iron-rich oxides along the chromite grain boundaries and silicate particles. Their role in the rate of intergranular corrosion is discussed.


*Keywords:* Atom probe tomography; Corrosion; Oxidation; Stainless steel; Chromium oxide spinels

For better efficiency, higher operating temperatures are required for thermal energy production technologies such as coal, nuclear, geothermal and solar thermal electric. This will lead to an increasing demand for affordable advanced high-temperature alloys. Austenitic stainless steels (ASSs) are the alloys of choice for high-temperature energy technologies that require a combination of affordability, strength and corrosion resistance. However, the high-temperature corrosion resistance of these stainless steels must be improved if it is to withstand the extreme operating conditions of new high-temperature technologies such as concentrated solar power (CSP), where temperatures can cycle from room temperature to up to 1000 °C [1]. For example, a recent study highlighted the failure of a commercial high-temperature ASS (253 MA) used as a CSP receiver via an oxidation-induced martensitic transformation associated with intergranular corrosion (IGC) [2]. The composition and structure of the intergranular scale formed during CSP operation play a significant role in the rate at which IGC progresses.

It is well established that Cr-rich oxide scales such as $Cr_2O_3$ or $FeCr_2O_3$ are more protective than Fe-rich oxide scales [3]. Numerous studies have characterized surface oxide scales formed in (Cr–Ni) ASS at high temperature in air [4,5]. These studies were carried out mainly by thermodynamic calculations and by using X-ray diffraction, spectroscopy techniques and analytical electron microscopy for microscale observations. Characterization of the intergranular oxide scale at an atomic level can provide additional insights useful for the development of alloys with improved high-temperature corrosion resistance. In the last decade, local electrode atom probe (LEAP) has also been applied to study oxide layers. For example, metallic oxide phases, such as wustite [6], hematite [7], chromia [8], as well as surface oxide layers in stainless steels or nickel-based alloys [9–11], have been characterized by using laser-pulsed LEAP. Here we use LEAP to reveal the atomic-scale structure of intergranular oxides that have formed in a commercial ASS (253 MA) used as a receiver in a CSP plant.

A Sandvik 253 MA ASS (Fe–0.08C–21–Cr–10.8Ni–1.64Si–0.58Mn–0.02P–0.44Cu–0.19Mo–0.06V–0.01Ti–0.17N–0.05Ce/La in wt.%) alloy was subjected to thermal cycles in air between room temperature up to 970 °C for four day-and-night cycles [2]. A cross-section of the tube was prepared by mechanically polishing for scanning electron microscopy. The oxides within the IGC region were analyzed by energy-dispersive X-ray spectroscopy (EDS) and electron backscatter diffraction (EBSD) on a Zeiss Ultra scanning electron microscope. APT samples were prepared from IGC layers using a Zeiss-Auriga focused ion beam (FIB) equipped with a Kleindiek micromanipulator system. Two bars of corrosion layers from two different IGC areas were lifted-out. Samples were milled from these bars, attached to electropolished molybdenum grids and finally milled to form APT tips [12]. The APT experiments were conducted on a Cameca LEAP 4000X Si™ atom probe equipped with a picosecond-pulse ultraviolet laser. The data were reconstructed using the Cameca software IVAS 3.6.6. The dataset shown in Figure 2 was collected at a

* Corresponding author at: School of Aerospace, Mechanical, Mechatronic Engineering, The University of Sydney, NSW 2006, Australia; e-mail: alex.lafontaine@sydney.edu.au

http://dx.doi.org/10.1016/j.scriptamat.2014.09.028
1359-6462/

temperature of 50 K, with a pulse energy of 75 pJ and a frequency of 250 kHz operating at an evaporation rate of 0.5%. The dataset shown in Figures 3 and 4 was collected at a temperature of 55 K, with a pulse energy of 40 pJ and a frequency of 500 kHz operating at an evaporation rate of 0.5%.

Scanning electron microscopy investigation of a cross-section of the receiver tube after 100 h of service revealed extensive IGC cracks penetrating beneath the surface of the tube by ~1.3 mm (Fig. 1a). This IGC is the result of sensitization [13,14] during thermal cycling. Sensitization leads to a depletion of Cr at the grain boundaries (GBs) such that a protective Cr-rich scale cannot be formed and the alloy is preferentially oxidized in and around the GBs. Based on previous studies in which similar alloys were oxidized in air at above 900 °C, possible oxide phases include a mix of spinels ($FeCr_2O_4$, $Fe_3O_4$, $Mn_{0.5}Cr_{0.5}O_4$, $SiO_2$) and corundum ($Cr_2O_3$–$Fe_2O_3$) [5,15]. Other studies have showed the formation of (Fe,Cr,Ni)O [16]. EBSD/EDS maps of a small area within a single IGC layer are shown in Figure 1b–d. The maps reveal that the primary oxide is the chromite-type oxide, $Fe(Fe,Cr)_2O_4$.The austenite phase is the stainless steel and the body-centered cubic layers are caused by oxidation-induced Cr depletion [2].

With a high Cr content, the 253 MA ASS has been designed to withstand high-temperature corrosion in various environments [17]. However, the Cr depletion due to sensitization along GBs leads to the formation of intergranular Fe–Cr spinels instead of the more protective $Cr_2O_3$ scale [3]. Moreover, some studies done on ASSs in

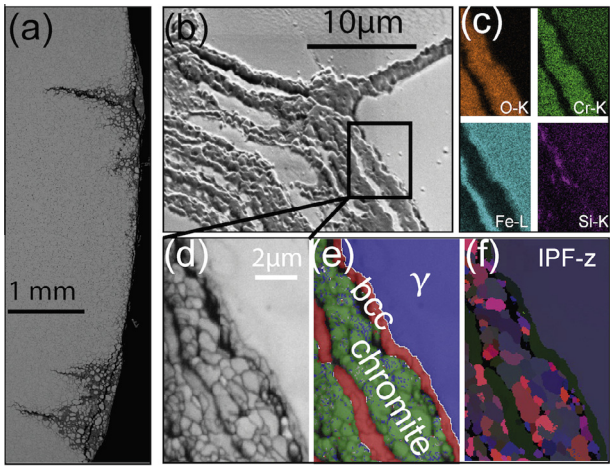


**Fig. 1.** Intergranular corrosion (IGC) in 253MA after thermal cycling. (a) Z-contrast backscattered electron image of a cross-section of the sample showing several large IGC cracks. (b) Secondary electron image of a section of an IGC area. The marked area shows where the EBSD/EDS mapping was done. (c) EDS O-*K*, Cr-*K*, Fe-*L* and Si-*K* maps. (d) EBSD pattern quality map. (e) EBSD phase map. (f) IPF-z orientation map. Note the multiple grains of chromite revealed by EBSD (d–e).

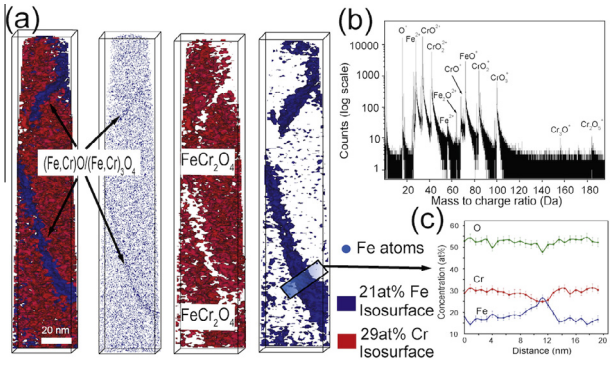


**Fig. 2.** APT reconstructed volumes of Fe-rich oxides within two chromite GBs. (a) Respectively, 29 at.% Cr and 21 at.% Fe isoconcentration map (6 nm slice of data), Fe atoms (3 nm slice), 29 at.% Cr isoconcentration map, and 21 at.% Fe isoconcentration map. (b) Indexed mass spectrum from the dataset (log scale). (c) Concentration profile across a chromite GB (volume marked in the Fe isoconcentration map in (a)).

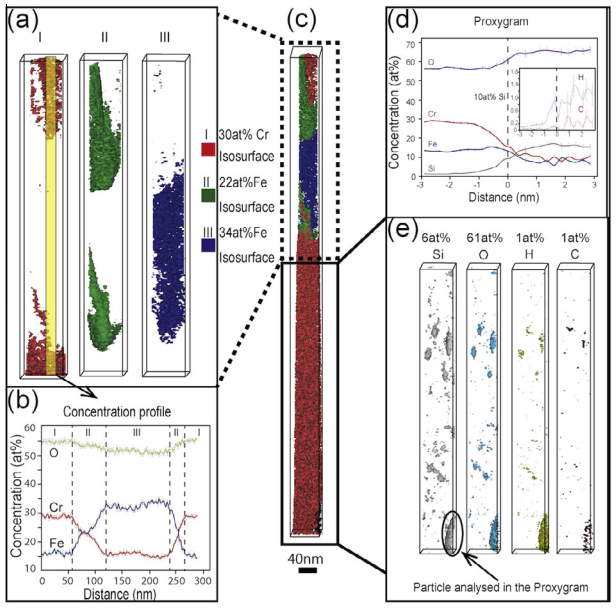


**Fig. 3.** APT reconstructed volumes of an IGC chromite layer containing Fe-rich oxides. (a) Isoconcentration maps of, respectively, 30 at.% Cr, 22 at.% Fe and 34 at.% Fe from the upper part of the reconstructed volume (dashed box). Zone I corresponds to chromite, zone II to a diffusion layer from chromite to Fe-rich oxide and zone III to a mix between ferrous oxide and Fe-rich spinel. (b) Concentration profile in the Z-direction across the upper part of the sample (see highlighted volume in (a)). Zones I, II and III are shown in the graph. (c) Isoconcentration maps of, respectively, 30 at.% Cr, 22 at.% Fe and 34 at.% Fe from the full reconstructed volume. (d) Proximity histogram (proxigram) analysis of a silicate particle (circled in (e)). (e) Isoconcentration maps of Si (6 at.%), O (61 at.%), H (1 at.%) and C (1 at.%) from the bottom part of the reconstructed volume.

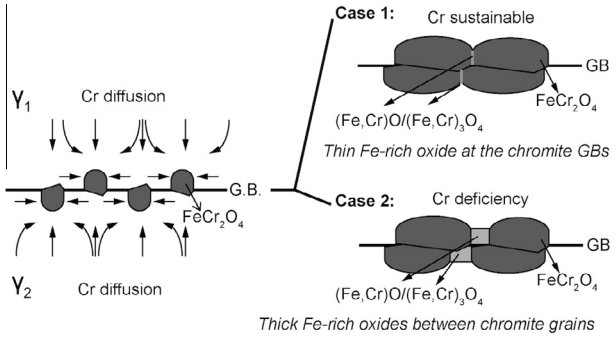


**Fig. 4.** Sketch showing the two proposed mechanisms for the formation of Fe-rich oxides within the chromite.